applied sciences

MDPI

Article

A Method for Expansion of Z-Directional Measurement Range in a Mode-Locked Femtosecond Laser Chromatic Confocal Probe

Chong Chen, Ryo Sato, Yuki Shimizu *, Taku Nakamura, Hiraku Matsukuma and Wei Gao

Precision Nanometrology Laboratory, Department of Finemechanics, Tohoku University, Sendai 980-8579, Japan; chongchen@nano.mech.tohoku.ac.jp (C.C.); satoryo@nano.mech.tohoku.ac.jp (R.S.); nakamura@nano.mech.tohoku.ac.jp (T.N.); hiraku.matsukuma@nano.mech.tohoku.ac.jp (H.M.); gaowei@cc.mech.tohoku.ac.jp (W.G.)

* Correspondence: yuki.shimizu@nano.mech.tohoku.ac.jp; Tel.: +81-22-795-6950

Received: 13 December 2018; Accepted: 22 January 2019; Published: 29 January 2019

Abstract: A method is proposed to expand the Z-directional measurement range of a fiber-based dual-detector chromatic confocal probe with a mode-locked femtosecond laser source. In the dual-detector chromatic confocal probe, the Z-directional displacement of a measurement target is derived from the peak wavelength in the normalized intensity ratio from the two light intensities obtained by the two identical fiber detectors. In this paper, a new method utilizing the main-lobe and side-lobes of axial responses acquired from both the normalized intensity ratio I_a and the invert normalized intensity ratio I_n, which is the inverse of I_a, is proposed to obtain the seamless relationship between the peak wavelength and the Z-directional displacement of a measurement target. Theoretical calculations and experimental investigation are carried out to demonstrate the feasibility of the proposed measurement range expansion method.

Keywords: chromatic confocal probe; femtosecond laser; measurement range expansion; side-lobe

1. Introduction

Confocal microscopy [1,2] with a confocal probe has outstanding image formation properties in depth sectioning imaging and optical tomographic imaging [3–5], which makes it a potentially powerful tool for image formation in industrial and medical engineering fields, such as three-dimensional (3D) fine structure image formation [4,5] and living body observation of cells [6,7], compared with traditional microscopy. It is also expected to measure large-area 3D microstructured surfaces [8,9]. Meanwhile, the relatively small measurement range of a confocal probe with a monochromatic laser source has prevented the further application of confocal microscopy in these areas. Therefore, the extension of the measurement range of a confocal probe is critical and crucial for expansion of the application range of the confocal microscopy. For the extension of the measurement range of a confocal probe, several efforts have already been made so far [10–20]. Among them, enhancement of the chromatic dispersion has been proven as a way to realize the extension of the measurement range without any axial scanning of a target object or a measuring head of a confocal probe [18–20]. The employment of a diffractive optical element (DOE) is a candidate method to enhance the chromatic aberration, and five-fold extension of measurement range has been achieved [10]. Other DOEs for enlargement of the chromatic dispersion, such as a micro-lens array [13] and a Fresnel lens [14], have achieved enlarged measurement ranges of 210 μm and 200 μm, respectively. With a diffractive lens and objective lenses [11], an expansion of a measurement range has also been achieved [11,16]. Furthermore, by utilizing a pupil filter technique, such as super-resolution pupil filter [15] or annular pupil filter [17], for the re-shaping of a measuring beam, measurement ranges have also been enlarged to 40 μm and 14 μm, respectively. However,

the above methods need to employ additional optical components in the optical setup, which could affect the performances of original optical confocal setups. Meanwhile, employing a broadband laser source is another approach to expand the measurement range of a chromatic confocal probe [18,19], and several methods have been proposed so far. With the employment of a supercontinuum laser source, over 16-fold expanded measurement range has been acquired [19]. However, non-smoothness of the laser spectrum, which means non-uniformity of the spectral intensity distribution, has restricted the full exploration of the whole spectrum of the supercontinuum laser source for a wider axial measurement range in a chromatic confocal probe. In responding to the background described above, a fiber-based dual-detector chromatic confocal probe with a mode-locked femtosecond laser source has been developed [3]. The proposed method has demonstrated that the influence of non-smoothness of the mode-locked femtosecond laser source can be compensated while expanding the measurement range over the whole spectrum of the laser by employing an axial response, defined as the intensity ratio of the two different confocal signals.

In this paper, as the second step of research, a new signal processing method for the axial response curve from the fiber-based dual-detector chromatic confocal probe with a mode-locked femtosecond laser source is proposed. The method is designed to further expand the measurement range without modifying the optical setup of the dual-detector chromatic confocal probe. Due to the diffraction effect of a point detector in confocal microscopy [20], there are always a main-lobe and side-lobes in the axial response of a confocal probe, in which main-lobe stands for the highest power intensity distribution curve of the axial response, while side-lobes stand for local maxima power intensity distribution curves of the axial response. Since the presence of the side-lobes not only reduces the light intensity of the main-lobe but also degrades the imaging quality and depth resolution of confocal microscopy, a variety of methods have been proposed so far to reduce [21–29], or even remove [30,31], the side-lobes in the axial response. On the contrary, in this paper, these annoying side-lobes are utilized to expand the measurement range of the dual-detector chromatic confocal probe with a mode-locked femtosecond laser source. Theoretical analysis and computer simulation, as well as some experiments, are carried out to demonstrate the feasibility of the proposed method for the extension of the measurement range.

2. Principle of the Extension of the Measurement Range

2.1. Imaging Principle

Figure 1 shows a schematic of the optical configuration for the fiber-based dual-detector chromatic confocal probe with a mode-locked femtosecond laser source [3]. A mode-locked femtosecond laser source is employed, while single-mode step index fibers are used as the signal-propagating media. The kth optical mode in the mode-locked femtosecond laser has a specific frequency ν_k, which corresponds to the deterministic working wavelength λ_k, which can be expressed as follows by using the carrier envelope offset frequency ν_{ceo} and the pulse repetition rate ν_{rep} [32–34]:

$$\nu_k = \nu_{\mathrm{ceo}} + k \cdot \nu_{\mathrm{rep}} \tag{1}$$

$$\lambda_{\mathrm{k}} = \frac{c}{\nu_k} \tag{2}$$

where c is the speed of light in vacuum. For the image formation of confocal microscopy, the point spread function (PSF), and the pupil function of imaging lens are critical and are used in the equation of the final axial response of the confocal microscopy. The equation of the PSF, pupil function, and the equation of the effective PSF are given as follows [3,35–37]:

$$h_i(u,v) = \int_0^1 P_i(u,\rho) J_0(\rho v) \rho d\rho, i = 1,2, \tag{3}$$

$$P_i = \begin{cases} 1, in\ pupil \\ 0, else \end{cases}, \quad i = 1,2 \tag{4}$$

$$h_{i\_\mathrm{eff}}(u,v) = h_i(u,v) \otimes e_1(u,v), \quad i = 1,2 \tag{5}$$

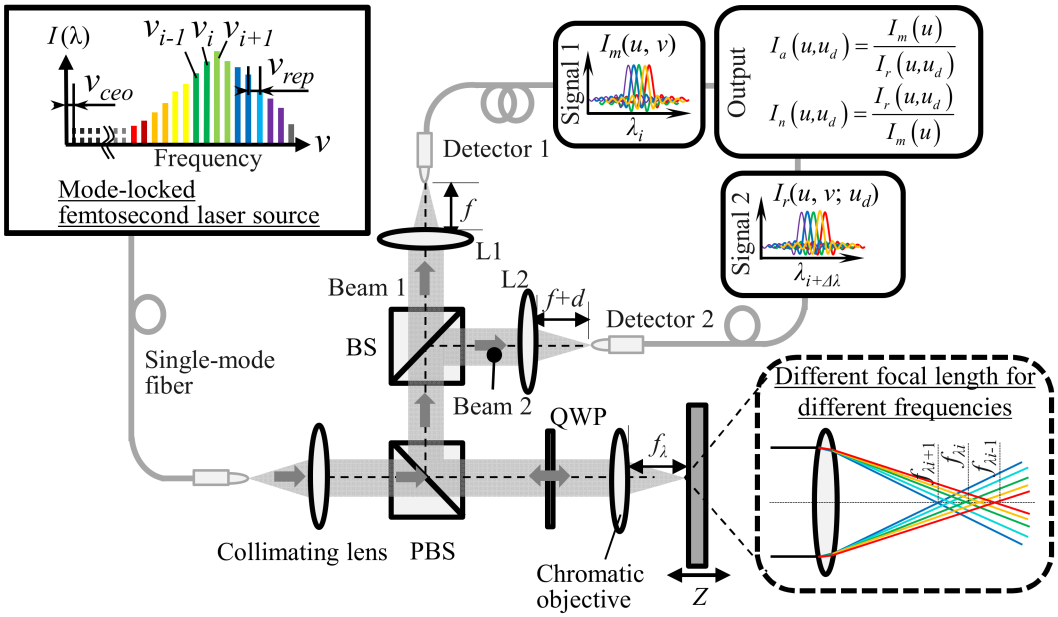

Figure 1. Schematic diagram of the fiber-based dual-detector chromatic confocal configuration with a mode-locked femtosecond laser source.

The complex amplitude U_f on the confocal plane is therefore given as follows:

$$U_f(u,v) = h_{1\_\mathrm{eff}}(u,v) h_{2\_\mathrm{eff}}(u,v) \otimes t(u,v) \tag{6}$$

where $h_i(u, v)$ and $P_i(u, \rho)$ are the PSF and the pupil function of the two imaging lenses, respectively, ρ being the normalized radius of the chromatic objective lens, $\otimes$ standing for the convolution operation, $J_0(\blacksquare)$ being the Bessel function of the first kind of zero order, h_{i_eff} standing for the effective PSF of the two imaging lenses, e_1 being the fundamental transverse orthonormal modal field. It should be noted that u and v are the optical coordinates of the confocal setup associated with the real coordinates z and r, respectively, and can be described by the following equations [3,36,37]:

$$v = \frac{2\pi}{\lambda} r \sin\beta \tag{7}$$

$$u = \frac{2\pi}{\lambda} z \sin^2\beta \tag{8}$$

where λ and $\sin\beta$ indicate the light wavelength and the numerical aperture of the chromatic objective lens, respectively. Since the whole confocal configuration is coherent, the light intensity I obtained by the detector placed on the focal plane of the objective lens is given by the following equation:

$$I = |h_{1\_\mathrm{eff}}(u,v) h_{2\_\mathrm{eff}}(u,v) \otimes t(u,v)|^2 \tag{9}$$

where $t\ (u, v)$ is the amplitude reflection or transmittance of the object. Based on the above analyses, the light intensity distribution $I_\mathrm{m}(u)$ on the focal plane of the objective lens, where the fiber detector is placed, is given as follows:

$$I_{\mathrm{m}}(u) = \left| \int_0^1 \exp\left(ju\rho^2\right) P_{1\_eff} P_{2\_eff} \rho d\rho \right|^2 \tag{10}$$

In order to overcome the non-smoothness of the laser spectrum in the mode-locked femtosecond laser source, a dual-detector differential confocal configuration shown in Figure 1 has been proposed [3]. The light intensity distribution $I_{\mathrm{r}}(u, u_d)$ on the plane with a distance d from the focal plane of the objective lens is given as follows:

$$I_{\mathrm{r}}(u, u_d) = \left| \int_0^1 \exp\left[j\left(u + \frac{u_d}{2}\right)\rho^2\right] P_{1\_eff} P_{2\_eff} \rho d\rho \right|^2 \tag{11}$$

where u_d is the optical distance associated with the defocus d that can be described as follows:

$$u_d = \frac{2\pi}{\lambda} d \sin^2 \beta \tag{12}$$

Figure 2a shows typical spectra of the light intensities $I_{\mathrm{m}}(u)$ and $I_{\mathrm{r}}(u, u_d)$ obtained by the two identical fiber detectors. As can be seen in the figure, it is difficult to distinguish a peak in the spectra, since a mode-locked femtosecond laser source has a non-smooth spectrum, as shown in Figure 2b. The spectrum shown in Figure 2b is from a specific femtosecond laser used in the following experiments and its non-smooth spectrum is not the same as the other generic laser sources. To address the aforementioned problem, the normalized intensity ratio $I_{\mathrm{a}}(u, u_d)$ and the invert normalized intensity ratio $I_{\mathrm{n}}(u, u_d)$ of the obtained signal intensities, determined by the following equations, are employed in the proposed method:

$$I_{\mathrm{a}}(u, u_d) = \frac{I_{\mathrm{m}}(u)}{I_{\mathrm{r}}(u, u_d)} \tag{13}$$

$$I_{\mathrm{n}}(u, u_d) = \frac{I_{\mathrm{r}}(u, u_d)}{I_{\mathrm{m}}(u)} \tag{14}$$

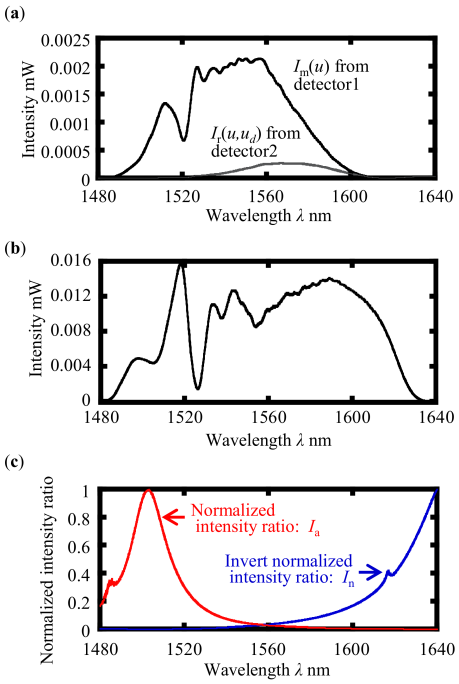

Figure 2. Typical normalized intensity ratio obtained by the dual-detector chromatic confocal configuration with a mode-locked femtosecond laser source. (**a**) Light intensities obtained by the two identical fiber detectors with a target position of 40 μm and a defocus d of 150 μm; (**b**) Working spectrum of the mode-locked femtosecond laser source; (**c**) Normalized intensity ratio and invert normalized intensity ratio obtained from the two light intensities.

Figure 2c shows the normalized intensity ratio and the invert normalized intensity ratio obtained from the spectra of the obtained light intensities shown in Figure 2a, with a target position of 40 μm and a defocus d of 150 μm, in which main-lobes can clearly be distinguished in both the normalized intensity ratio I_{a} and the invert normalized intensity ratio I_{n}, but side-lobes are inconspicuous. Therefore, in subsequent simulations and experiments, to make good use of the side-lobes to extend the measurement range, we set a defocus d to be 110 μm so that the side-lobes can be visible. As can be seen in the figure, main peaks can clearly be distinguished in both the axial response and the reversed axial response; this enables the proposed fiber-based dual-detector chromatic confocal probe to have a high resolution of 30 nm and good linearity for displacement measurement along the depth direction.

2.2. Expansion of the Measurement Range

The measurement range of the proposed fiber-based dual-detector chromatic confocal probe is determined by the spectral bandwidth of the mode-locked laser source and the chromatic objective employed in the optical setup. A thin plano-convex lens made of N-SF11 is employed in the developed optical setup as the chromatic objective. According to the thin-lens equation [3,35], the relationship between a focal length of the chromatic objective f_λ and a refractive index N_λ is given as follows:

$$f_\lambda = \frac{1}{(N_\lambda - 1)(1/r_1 - 1/r_2)} \tag{15}$$

where r_1 and r_2 are curvature radii of the chromatic objective lens. The refractive index N_λ for the light wavelength λ can be obtained from the following Sellmeier equation [3]:

$$N_\lambda = \sqrt{1 + \frac{B_1\lambda^2}{\lambda^2 - C_1} + \frac{B_2\lambda^2}{\lambda^2 - C_2} + \frac{B_3\lambda^2}{\lambda^2 - C_3}} \tag{16}$$

where B_i and C_i are the parameters associated with N-SF11. The measurement range ΔZ of the chromatic confocal probe is therefore given as follows:

$$\Delta Z = |f_{\lambda 1} - f_{\lambda 2}| \tag{17}$$

where $f_{\lambda 1}$ and $f_{\lambda 2}$ are the longest and shortest working wavelengths of the mode-locked femtosecond laser source, respectively. In the previous work by the authors [3], the measurement range of the developed chromatic confocal probe is derived from the linear relationship between the target position and the peak wavelength detected in the normalized intensity ratio.

To further expand the measurement range of the fiber-based dual-detector chromatic confocal probe without any modifications on the optical setup, in this paper, a new method employing both the main-lobes and the side-lobes of the axial responses obtained from the normalized intensity ratio I_{a} (u, u_d) and the invert normalized intensity ratio I_{n} (u, u_d) is proposed. Figure 3 shows a variation of the normalized intensity I_{a} as a function of the Z-directional position of a measurement target at a specific wavelength λ, which is referred to as the axial response [3]. Figure 3 also shows the axial response obtained from the invert normalized intensity ratio at the same wavelength λ. As can be seen in the figures, not only the main-lobes but also the side-lobes of the axial response proposed in our previous work [3], which cannot be observed in the single axial responses of I_{m} and I_{r} without the normalization process, can clearly be distinguished in the axial responses. This is another benefit of our newly proposed axial response; the side-lobes are clearer compared with the single axial response expected from a Lorentzian shape, in which the side-lobe is fuzzy and cannot be identified easily. Figure 4a–c show the normalized intensity ratio I_{a} (u, u_d) and the invert normalized intensity ratio $I_{\mathrm{n}}(u, u_d)$ with different defocus d, and Figure 4d shows the side-lobe spacing and the main-lobe to side-lobe spacing with respect to different defocus d. In order to make good use of the side-lobes to extend the measurement range, we set defocus d to be 110 μm, in which the side-lobes are more

visible and identifiable than the cases where d is set to be within a range from 50 μm to 80 μm. Consequently, the employment of the side-lobes has a possibility of expanding the measurement range of the fiber-based dual-detector chromatic confocal probe, and theoretical calculations are therefore carried out in the following.

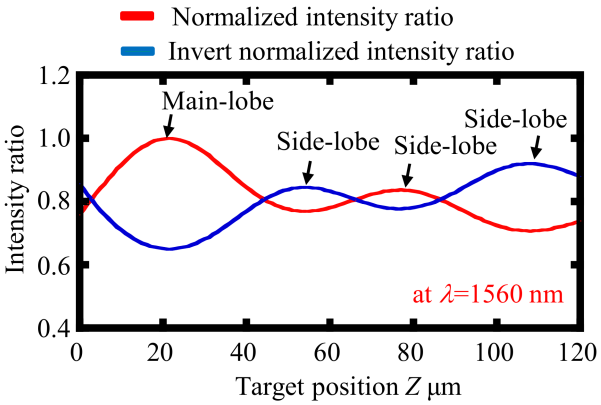

Figure 3. A typical axial response obtained by the dual-detector chromatic confocal probe with a mode-locked femtosecond laser source with axial response of the normalized intensity ratio and axial response of the invert normalized intensity ratio, with target positions ranging from 0 to 120 μm and a defocus d of 110 μm.

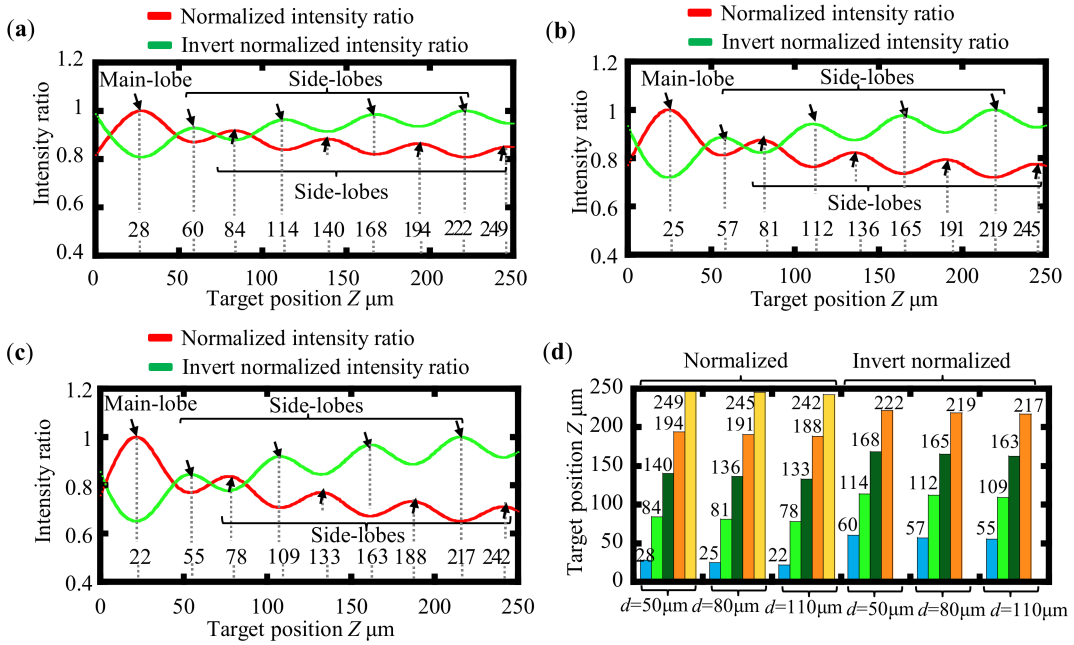

Figure 4. The main-lobes and the side-lobes extracted from the normalized intensity ratio and the invert normalized intensity ratio obtained at central wavelength λ = 1560 nm, together with side-lobe spacing and main-lobe to side-lobe spacing with target positions ranging from 0 to 250 μm and defocus d ranging 50 μm to 110 μm. (**a**) Main-lobe and side-lobes obtained from normalized and invert normalized intensity ratio at central wavelength with d = 50 μm. (**b**) Main-lobe and side-lobes obtained from normalized and invert normalized intensity ratio at central wavelength with d = 80 μm. (**c**) Main-lobe and side-lobes obtained from normalized and invert normalized intensity ratio at central wavelength with d = 110 μm. (**d**) The side-lobe spacing and main-lobe to side-lobe spacing at central wavelength with d = 50 μm, 80 μm, and 110 μm.

Regarding the non-smoothness of the laser spectrum shown in Figure 2b, axial responses of the fiber-based dual-detector chromatic confocal probe are estimated based on Equations (13) and (14), in

which the proposed axial response is defined as the intensity ratio of the signal 1 and signal 2, not as the single axial response anymore. The distance between the main-lobe and the side-lobe is therefore determined by the relative magnitude of the ratios of signal 1 and signal 2 at the same target position. Furthermore, the relative height of the main-lobe and the side-lobes is also controlled by the relative magnitude of the ratios of signal 1 and signal 2 at the same target position, which is further controlled by the defocus d that is shown in Equation (11). As illustrated in Equation (11), when we set a defocus d to be zero, theoretically the values of Equation (13) and Equation (14) always become 1.

For the calculations, the parameters summarized in Table 1 are employed to express the effect of the chromatic objective. Figure 5a,b show the axial responses from the normalized intensity ratio and the invert normalized intensity ratio, respectively, calculated at the wavelengths from 1550 nm to 1580 nm. As can be seen in the figures, the main-lobe and the side-lobes of the axial response from the invert normalized intensity ratio are found to be shifted along the axial (Z-) direction with respect to those from the normalized intensity ratio. In the previous work by the authors [3], only the information from the main-lobe in the normalized intensity ratio has been employed to detect a displacement in the axial direction. As a result, the measurement range has been limited to be approximately 40 μm. Meanwhile, by using the information from not only the main-lobe but also the side-lobes in the axial responses from both the intensity ratios, the measurement range can be expanded; as can be seen in Figure 5c, the gap of the neighboring lobes (including the main-lobe and side-lobes) in the axial response of $I_a(u, u_d)$ can be covered by the corresponding lobes of the axial response of $I_n(u, u_d)$.

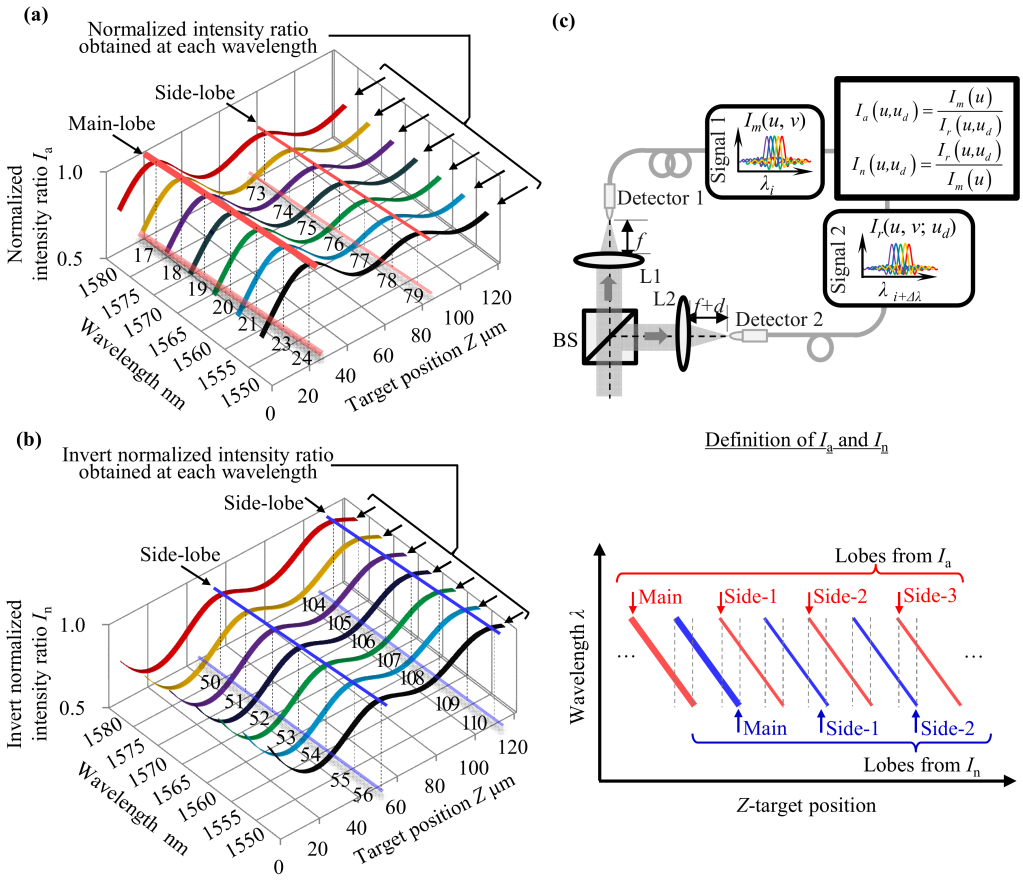

Figure 5. The main-lobe and the side-lobes in the axial response obtained by the dual-detector chromatic confocal probe with a mode-locked femtosecond laser source with target positions ranging from 0 to 120 μm and a defocus d of 110 μm. (**a**) Axial response of the normalized intensity ratio with shadow of the main-lobe and side-lobe and the corresponding target position values. (**b**) Axial response of the invert normalized intensity ratio with shadow of the side-lobes and the corresponding target position values. (**c**) The main-lobes and the side-lobes in the axial responses.

Table 1. Parameters employed for the theoretical calculation.

Items		Symbol	Value
Lens material		-	N-SF11
Surface radii of imaging lens		r_1	7.85 mm
		r_2	∞
	Sellmeier coefficients		
B_1	1.73759695	C_1	0.013188707
B_2	0.313747346	C_2	0.062306814
B_3	1.89878101	C_3	155.23629

Theoretical calculation is expanded to a working range of the mode-locked laser of 1.48 μm–1.64 μm and a target position over 250 μm. Figure 6a,b show the axial responses of the normalized intensity ratio I_a and the invert normalized intensity ratio I_n. As can be seen in the figure, side-lobes are clearly observed over a target position range of 250 μm in both of the axial responses. Meanwhile, the existence of a gap between each neighboring lobes is also confirmed in both of the axial responses. In addition, the theoretical calculation results show that the gap becomes wider as the increase of the target position. Figure 6c shows the main-lobes and the side-lobes of the normalized intensity ratio I_a plotted together with those of the invert normalized intensity ratio I_n. As can be seen in the figure, the two axial responses are almost 180° out of phase, and the gaps between each neighboring lobes in the axial response of the normalized intensity ration can be covered by the lobes in the axial response of the invert normalized intensity ratio over a target position range of 150 μm.

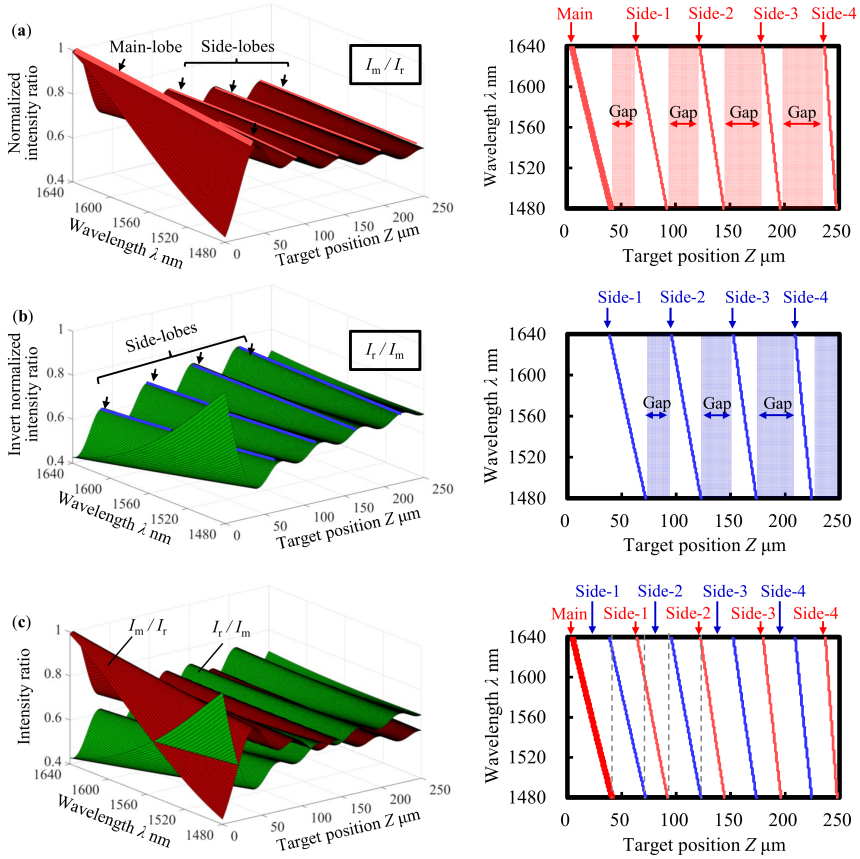

Figure 6. The main-lobe and the side-lobes in the axial responses obtained by the dual-detector chromatic confocal probe with a mode-locked femtosecond laser source. (**a**) Axial response of the normalized intensity ratio with target positions ranging from 0 to 250 μm and a defocus d of 110 μm. (**b**) Axial response of the invert normalized intensity ratio. (**c**) The main-lobes and the side-lobes in the axial responses.

It should be noted that in order to utilize the side-lobes of the axial responses as illustrated in Figure 6c for the expansion of the axial measurement range, calculation of partial derivatives of Equation (13) is necessary:

$$\frac{\partial I_a}{\partial z} = \frac{\partial I_a}{\partial u}\frac{\partial u}{\partial z} = \frac{4\pi \sin^2\beta\left\{ I_r\sqrt{I_m}\exp\left(ju\rho^2\right) - I_m\sqrt{I_r}\exp\left[j\left(u+\frac{u_d}{2}\right)\rho^2\right]\right\}}{{I_r}^2\lambda} \tag{18}$$

In order to obtain the relative maximum intensity values for wavelength-to-displacement encoding of the side-lobes, let Equation (13) be equal to zero and get the relationship between the target position z and wavelength λ:

$$\frac{\partial I_a}{\partial z} = \frac{\partial I_a}{\partial u}\frac{\partial u}{\partial z} = 0 \tag{19}$$

As illustrated in Figure 6c, the main-lobe and side-lobes are employed in the wavelength-to-displacement encoding, but gaps between main-lobe and side-lobes make the final measurement range discontinuous. In order to eliminate the gaps, side-lobes of the axial response of the invert normalized intensity ratio are employed. Therefore, the following relationship should also be satisfied:

$$\frac{\partial I_n}{\partial z} = \frac{\partial I_n}{\partial u}\frac{\partial u}{\partial z} = 0 \tag{20}$$

3. Experiments and Discussions

3.1. Experimental Setup

Figure 7 shows a schematic of the fiber-based dual-detector chromatic confocal probe developed in the previous study by the authors [3]. A mode-locked femtosecond laser (C-Fiber, MenloSystems) with a repetition rate ν_{rep} of 100 MHz and a spectral range of 1480–1640 nm was employed as the light source. Single-mode step index fibers were employed for the light propagation and for the detectors together with an optical spectrum analyzer (AQ6370D, Yokogawa Electric Corp.). The laser beam from the laser source was transmitted through the single-mode step index fiber, and the output laser beam from the fiber was then collimated by a collimating lens to generate a collimated beam with a beam diameter of approximately 3.6 mm. The collimated laser beam was then made to pass through a polarized beam splitter (PBS) and a quarter wave plate (QWP). By utilizing a chromatic objective (Edmund Optics, #67-484), the collimated laser beam was focused on a plane mirror mounted on a one-axis piezoelectric (PZT) positioning stage. The combination of the PBS and the QWP made sure that the light source was effectively isolated from the laser beam reflected from the plane mirror. A capacitance displacement sensor, whose measurement axis was aligned to coincide with the laser axis, was located behind the plane mirror to measure the target position of the mirror along the Z-direction. The propagating direction of the reflected laser beam was then bent 90 degrees by the PBS and was divided into two sub-beams by a non-polarizing beam splitter (BS). By utilizing an achromatic lens L1 with a focal length f of 16.6 mm, one of the sub-beams (sub-beam1) was coupled into one end face of a single-mode step index fiber, having a core diameter of 8.2 μm and a numerical aperture (NA) of 0.14. The other end face of the fiber was connected to the optical spectrum analyzer. Meanwhile, another sub-beam (sub-beam2) was coupled into one end face of another single-mode step index fiber, which was identical to that for the sub-beam1, by using another achromatic lens L2 identical to L1. It should be noted that the end face of the fiber for sub-beam2 was mounted on a precision manual stage system to give a defocus d to the end face of the fiber, with respect to the back focal plane of L2.

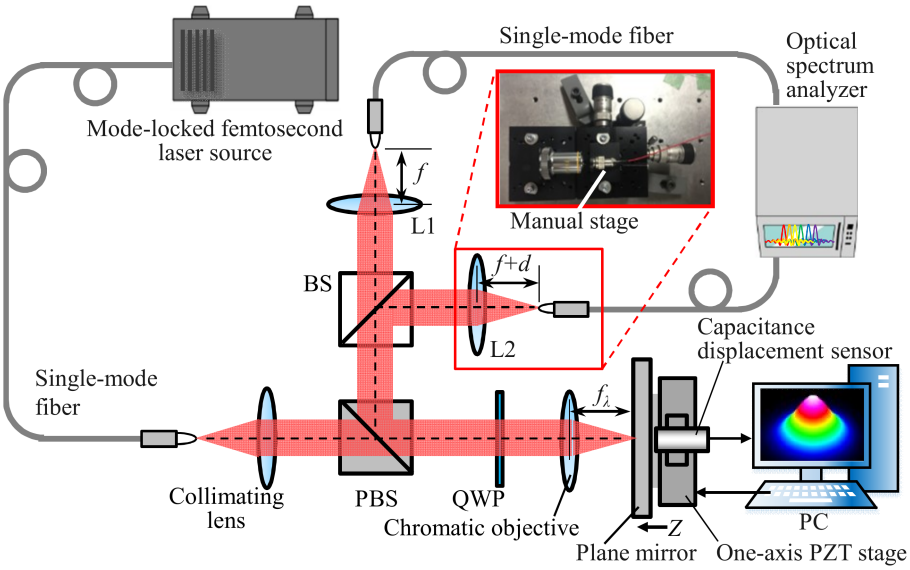

Figure 7. A schematic of the setup for the dual-detector chromatic confocal probe with a mode-locked femtosecond laser source.

3.2. Experiments

Experiments were carried out to investigate the feasibility of the proposed measurement range expansion method. The plane mirror was made to move along the *Z*-direction in a step of 2 μm to obtain the axial responses. It should be noted that the displacement of the plane mirror was measured by a capacitive displacement sensor simultaneously for comparison. Peak wavelengths were calculated from the centroid positions of the corresponding normalized intensity ratio, as well as the invert normalized intensity ratio at each *Z*-position of the mirror. Figure 8a shows the normalized intensity ratio obtained at each *Z*-position over a Z-directional scanning range of 250 μm. As can be seen in Figure 8a, not only the main-lobe but also the side-lobes were clearly observed. Although the peak widths of the sub-lobes were found to become wider as the increase of the *Z*-displacement of the plane mirror, the sharpness of the sub-lobes was enough to be used in the wavelength-to-displacement encoding. Figure 8b shows the peak wavelength obtained from the normalized intensity ratio in Figure 8a at each Z-directional position of the plane mirror. As can be seen in the figure, a linear relationship between the peak wavelength and the axial Z-directional displacement of the plane mirror was found for the main-lobe and each of the side-lobes. Meanwhile, as predicted in the results of the above theoretical calculations, a gap between each of the neighboring lobes was found. Figure 8c shows the invert normalized intensity ratio obtained at each *Z*-position, which was calculated from the same intensities employed to calculate the corresponding normalized intensity ratio shown in Figure 8a. As can be seen in Figure 8c, the main-lobe and the side-lobes were clearly observed in the obtained invert normalized intensity ratio. In the same manner, as the case of normalized intensity ratio I_a, the relationship between the peak wavelength and the axial *Z*-directional displacement of the flat mirror was investigated by extracting the peak wavelengths in the invert normalized intensity ratio I_n shown in Figure 8c. The result is summarized in Figure 8d. As predicted in the results of the above theoretical calculations, the peak frequency in the invert normalized intensity ratio at a specific Z-directional position of the plane mirror was found to shift along the axial direction with respect to that of the normalized intensity ratio shown in Figure 8b.

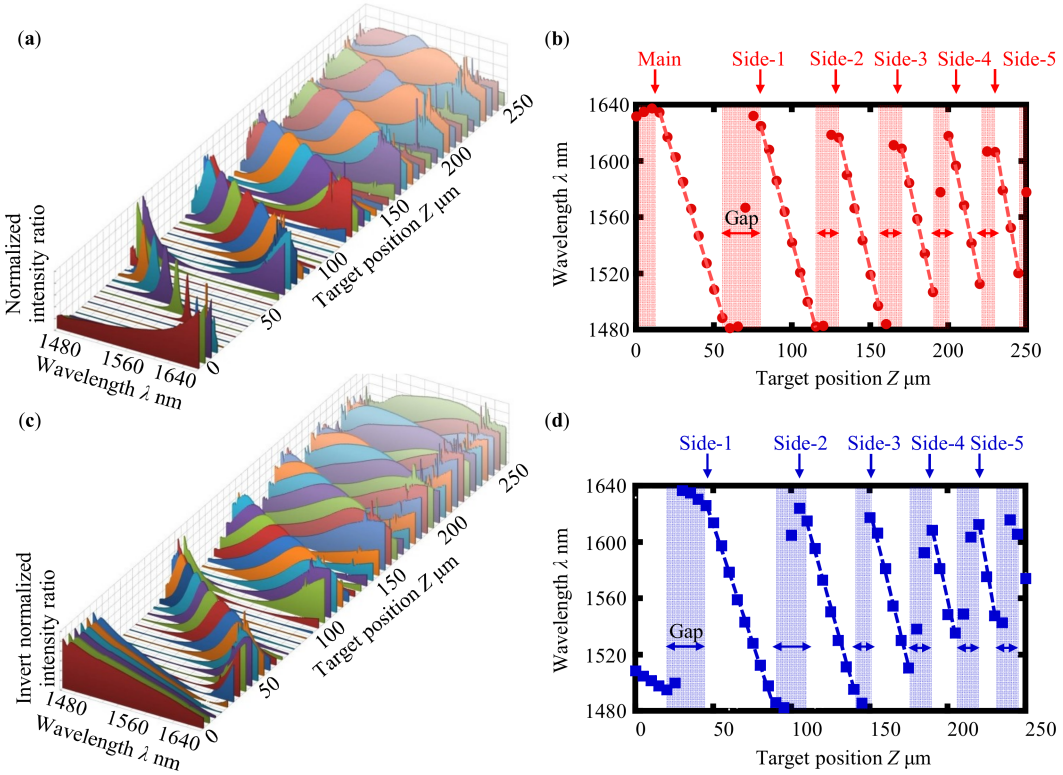

Figure 8. The main-lobes and the side-lobes extracted from the normalized intensity ratio and the invert normalized intensity ratio obtained at each Z-directional position of the plane mirror, with target positions ranging from 0 to 250 μm and a defocus d of 110 μm. (**a**) Normalized intensity ratio obtained at each Z-position over scanning range of 250 μm. (**b**) The lobes extracted from the normalized intensity ratio. (**c**) Invert normalized intensity ratio obtained at each Z-position over scanning range of 250 μm. (**d**) The lobes extracted from the invert normalized intensity ratio.

Figure 9 summarizes the wavelength-to-displacement encoding curves obtained from the axial responses of the normalized intensity ratio I_a and that of the invert normalized intensity ratio I_n. As can be seen in the figure, a gap between each neighboring lobe in the axial response of the normalized intensity ratio was successfully covered by the axial response from the invert normalized intensity ratio. These experimental results demonstrated that measurement range of the fiber-based dual-detector chromatic confocal probe was successfully expanded from 40 μm to 250 μm by the proposed method without any modification on the optical setup of the developed confocal probe.

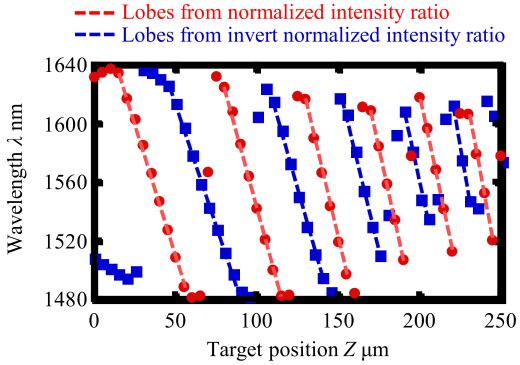

Figure 9. Wavelength-to-displacement encoding curves obtained from the axial responses of the normalized intensity ratio and that of the invert normalized intensity ratio, with target positions ranging from 0 to 250 μm and a defocus d of 110 μm.

4. Conclusions

A new method for expanding the Z-directional measurement range of a fiber-based dual-detector chromatic confocal probe with a mode-locked femtosecond laser source has been proposed. The dual-detector chromatic confocal probe has been designed to detect the axial position of a measurement target by using the normalized intensity ratio calculated from light intensities obtained by the two identical fiber detectors. In the proposed method, for the expansion of the measurement range of the dual-detector chromatic confocal probe, invert normalized intensity ratio, which is the inverse of the normalized intensity ratio, has also been employed to realize seamless measurement with the main-lobes and the side-lobes of the axial responses obtained from both the normalized intensity ratio and the invert normalized intensity ratio. Theoretical calculations and experiments have been carried out to verify the feasibility of the proposed method, and the results have demonstrated that the measurement range can be expanded to 250 μm, which is four times wider than that of the conventional dual-detector chromatic confocal probe developed in the previous work by the authors.

It should be noted that this paper is mainly focused on the proposal of the method for expansion of the Z-directional measurement, and subsequent experimental work will be carried out in 3D microstructure imaging in our future research. It should also be pointed out that in order to make good use of the side-lobes to extend the Z-directional measurement range, we set a defocus d to be 110 μm, which achieves a bigger full width at half maximum (FWHM) value compared with the FWHM value when the defocus d is set to be 150 μm in our previous work [3]. That means there will be a reduction in axial resolution. However, when the defocus d is fixed, the axial resolution will not be affected during the measurement range expansion processing because our expansion method is performed without modifying the optical setup of the dual-detector chromatic confocal probe, and therefore will not change the point spread function of our confocal imaging system theoretically. Furthermore, future research will also focus on the depth measurement provided by the optical phase and optical complex amplitude of the dual-detector chromatic confocal probe, compared with the depth measurement given by the optical intensity in this paper. Measurement uncertainty analysis together with the identification of the absolute optical wavelengths based on the optical frequency comb will also be carried out in the next stage of research.

Author Contributions: Conceptualization, W.G.; methodology, C.C. and T.N.; software, C.C. and T.N.; validation, C.C., H.M., and R.S.; formal analysis, C.C., T.N., and R.S.; investigation, C.C., T.N., and R.S.; resources, C.C. and R.S.; data curation, C.C. and R.S.; writing—original draft preparation, C.C.; writing—review and editing, Y.S., H.M., and C.C.; visualization, W.G. and Y.S.; supervision, W.G.; project administration, W.G.; funding acquisition, W.G. and Y.S.

Funding: This research was funded by Japan Society for the Promotion of Science (JSPS).

Conflicts of Interest: The authors declare no conflict of interest. The funders had no role in the design of the study; in the collection, analyses, or interpretation of data; in the writing of the manuscript, and in the decision to publish the results.

References

1. Gao, W.; Kim, S.W.; Bosse, H.; Haitjema, H.; Chen, Y.L.; Lu, X.D.; Knapp, W.; Weckenmann, A.; Estler, W.T.; Kunzmann, H. Measurement technologies for precision positioning. *CIRP Ann. Manuf. Technol.* **2015**, *64*, 773–796. [CrossRef]
2. Butler, D.; Horsfall, A.; Hrynevych, M.; Kearney, P.D.; Nugent, K.A. Confocal profilometer with nanometric vertical resolution. *Opt. Commun.* **1993**, *100*, 87–92. [CrossRef]
3. Chen, X.G.; Nakamura, T.; Shimizu, Y.; Chen, C.; Chen, Y.L.; Matsukuma, H.; Gao, W. A chromatic confocal probe with a mode-locked femtosecond laser source. *Opt. Laser Technol.* **2018**, *103*, 359–366. [CrossRef]
4. Chen, L.C.; Chang, Y.W. Innovative simultaneous confocal full-field 3D surface profilometry for in situ automatic optical inspection (AOI). *Meas. Sci. Technol.* **2013**, *21*, 1–12.

5. Bohn, S.; Sperlich, K.; Allgeier, S.; Bartschat, A.; Prakasam, R.; Reichert, K.M.; Stolz, H.; Guthoff, R.; Mikut, R.; Kohler, B.; et al. Cellular in vivo 3D imaging of the cornea by confocal laser scanning microscopy. *Biol. Opt. Express* **2018**, *9*, 2511–2525. [CrossRef] [PubMed]
6. Stephens, D.J.; Allan, V.J. Light Microscopy Techniques for Live Cell Imaging. *Science* **2003**, *300*, 82–86. [CrossRef] [PubMed]
7. Hickey, P.C.; Swift, S.R.; Roca, M.G.; Read, N.D. Live-cell imaging of filamentous fungi using vital fluorescent dyes and confocal microscopy. *Methods Microbiol.* **2004**, *34*, 63–87.
8. Gao, W.; Araki, T.; Kiyono, S.; Okazaki, Y.; Yamanaka, M. Precision nano-fabrication and evaluation of a large area sinusoidal grid surface for a surface encoder. *Precis. Eng.* **2003**, *27*, 289–298. [CrossRef]
9. Shimizu, Y.; Aihara, R.; Mano, K.; Chen, C.; Chen, Y.L.; Chen, X.; Gao, W. Design and testing of a compact non-orthogonal two-axis Lloyd's mirror interferometer for fabrication of large-area two-dimensional scale grating. *Precis. Eng.* **2018**, *52*, 138–151. [CrossRef]
10. Berkovic, G.; Shafira, E.; Golubb, M.A.; Brilb, M.; Shurmanb, V. Multi-wavelength fiber-optic confocal position sensor with diffractive optics for enhanced measurement range. *Proc. SPIE* **2007**, *6619*, 66190U.
11. Dobson, S.L.; Sun, P.C.; Fainman, Y. Diffractive lenses for chromatic confocal imaging. *Appl. Opt.* **1997**, *36*, 4744–4748. [CrossRef] [PubMed]
12. Shafir, E.; Berkovic, G. Expanding the realm of fiber optic confocal sensing for probing position, displacement, and velocity. *Appl. Opt.* **2006**, *45*, 7772–7777. [CrossRef] [PubMed]
13. Tiziani, H.J.; Achi, R.; Kramer, R.N. Chromatic confocal microscopy with microlenses. *J. Mod. Opt.* **1995**, *43*, 155–163. [CrossRef]
14. Garzon, R.J.; Meneses, J.; Tribillon, G.; Gharbi, T.; Plata, A. Chromatic confocal microscopy by means of continuum light generated through a standard single-mode fibre. *J. Opt. A Pure Appl. Opt.* **2004**, *6*, 544–548.
15. Zhao, W.Q.; Tan, J.B.; Qiu, L.R. Bipolar absolute differential confocal approach to higher spatial resolution. *Opt. Exp.* **2004**, *12*, 5013–5021. [CrossRef]
16. Lin, D.J.; Liu, Z.Y.; Zhang, R.; Yan, J.Q.; Yin, C.Y.; Xu, Y. Step-height measurement by means of a dual-frequency interferometric confocal microscope. *Appl. Opt.* **2004**, *43*, 1472–1479. [CrossRef] [PubMed]
17. Zhao, W.Q.; Tan, J.B.; Qiu, L.R. Improvement of confocal microscope performance by shaped annular beam and heterodyne confocal techniques. *Optik* **2005**, *116*, 111–117. [CrossRef]
18. Tan, J.B.; Liu, J.; Wang, Y.H. Differential confocal microscopy with a wide measuring range based on polychromatic illumination. *Meas. Sci. Technol.* **2010**, *21*, 1–6. [CrossRef]
19. Shi, K.B.; Nam, S.H.; Li, P.; Yin, S.Z.; Liu, Z.W. Wavelength division multiplexed confocal microscopy using supercontinuum. *Opt. Commun.* **2006**, *263*, 156–162. [CrossRef]
20. Zhao, W.Q.; Jiang, Q.; Qiu, L.R.; Liu, D.L. Dual-axes differential confocal microscopy with high axial resolution and long working distance. *Opt. Commun.* **2011**, *284*, 15–19. [CrossRef]
21. Sheppard, C.J.R.; Gu, M. Aberration compensation in confocal microscopy. *Appl. Opt.* **1991**, *30*, 3563–3568. [CrossRef] [PubMed]
22. Martinez-Corral, M.; Caballero, M.T.; Pons, A.; Andres, P. Sidelobe decline in single-photon 4Pi microscopy by Toraldo rings. *Micron* **2003**, *34*, 319–325. [CrossRef]
23. Suhre, D.R.; Gupta, N. Acousto-optic tunable filter sidelobe analysis and reduction with telecentric confocal optics. *Appl. Opt.* **2005**, *47*, 5797–5801. [CrossRef]
24. Segawa, S.; Kozawa, Y.; Sato, S. Resolution enhancement of confocal microscopy by subtraction method with vector beams. *Opt. Lett.* **2014**, *39*, 3118–3121. [CrossRef]
25. Nagorni, M.; Hell, S.W. 4Pi-Confocal microscopy provides three-dimensional images of the microtubule network with 100- to 150-nm resolution. *J. Struct. Biol.* **1998**, *123*, 236–247. [CrossRef] [PubMed]
26. Cox, I.J.; Sheppard, C.J.R.; Wilson, T. Improvement inresolution by nearly confocal microscopy. *Appl. Opt.* **1982**, *21*, 778–781. [CrossRef] [PubMed]
27. Brakenho, G.J.; Blom, P.; Barend, P. Confocal scanning light microscopy with high aperture immersion lenses. *J. Microsc.* **1979**, *117*, 219–232. [CrossRef]
28. Neil, M.A.A.; Juskaitis, R.; Wilson, T.; Laczik, Z.J. Optimized pupil-plane filters for confocal microscope point-spread function engineering. *Opt. Lett.* **2000**, *25*, 245–247. [CrossRef]
29. Wang, T.D.; Contag, H.C.; Mandella, M.J.; Chan, N.Y.; Kino, G.S. Dual-axes confocal microscopy with post-objective scanning and low-coherence heterodyne detection. *Opt. Lett.* **2003**, *28*, 1915–1917. [CrossRef]

30. Gweon, D.G.; Daejeon.; Kang, D.K. Confocal Self-Interference Microscopy from Which Side-Lobe Has Been Removed. U.S. Patent No. 7324.273 B2, 29 January 2008.
31. Stelzer, E.H.K.; Lindek, S. Fundamental reduction of the observation volume in far-field light microscopy by detection orthogonal to the illumination axis: Confocal theta microscopy. *Opt. Commun.* **1994**, *111*, 536–547. [CrossRef]
32. Jones, D.; Diddams, S.A.; Ranka, J.K.; Stentz, A.; Windeler, R.S.; Hall, J.L.; Cundiff, S.T. Carrier-envelope phase control of femtosecond mode-locked lasers and direct optical frequency synthesis. *Science* **2000**, *288*, 635–639. [CrossRef] [PubMed]
33. Chen, Y.L.; Shimizu, Y.; Kudo, Y.; Ito, S.; Gao, W. Mode-locked laser autocollimator with an expanded measurement range. *Opt. Exp.* **2016**, *24*, 15554–15569. [CrossRef] [PubMed]
34. Shimizu, Y.; Kudo, Y.; Chen, Y.L.; Ito, S.; Gao, W. An optical lever by using a mode-locked laser for angle measurement. *Precis. Eng.* **2017**, *47*, 72–80. [CrossRef]
35. Wilson, T.; Sheppard, C. *Theory and Practice of Scanning Optical Microscopy*; Academic Press: London, UK, 1984; pp. 17–20.
36. Wilson, T.; Carlini, A.R. Size of the detector in confocal imaging systems. *Opt. Lett.* **1987**, *12*, 227–229. [CrossRef] [PubMed]
37. Kimura, S.; Wilson, T. Confocal scanning optical microscope using single-mode fiber for signal detection. *Appl. Opt.* **1991**, *30*, 2143–2149. [CrossRef] [PubMed]